Mapping and monitoring peatlands in the Belgian Hautes Fagnes: Insights from Ground-penetrating radar and Electromagnetic induction characterization

Maud Henrion [a,b,*], Yanfei Li [b], Triven Koganti [c], Michel Bechtold [d], François Jonard [e], Sophie Opfergelt [a], Veerle Vanacker [b], Kristof Van Oost [b], Sébastien Lambot [a]

[a] Earth and Life Institute (Environmental Sciences), Université catholique de Louvain, 1348 Louvain-la-Neuve, Belgium
[b] Earth and Life Institute (Earth and Climate), Université catholique de Louvain, 1348 Louvain-la-Neuve, Belgium
[c] Department of Agroecology, Aarhus University, 8830 Tjele, Denmark
[d] Department of Earth and Environmental Sciences, KU Leuven, 3000 Leuven, Belgium
[e] Earth Observation and Ecosystem Modelling Laboratory, SPHERES Research unit, Université de Liège, 4000 Liège, Belgium

ABSTRACT

Peatlands are vital ecosystems providing crucial ecological services such as significant carbon storage in the context of climate change. These sensitive ecosystems are subjected to degradation due to land use change. In this context, it is important to understand the actual state of degraded peatlands and their recovery potential for regaining important functions. This study focuses on a disturbed peatland in the Belgian Hautes Fagnes, previously drained and planted with spruce, and characterized by a topographic gradient. We aimed to elucidate the use of Ground-penetrating radar (GPR) and Electromagnetic induction (EMI) techniques in characterizing such peatlands, with a specific focus on their implications for peat depth and electrical conductivity assessment, related to peatland degradation. The GPR revealed a high spatial heterogeneity in peat depth, ranging from 0.2 to more than 2 m on the site. In contrast, an EMI instrument used with single coil spacing proved to be unsuccessful to deduce peat depth but demonstrated potential for the delineation of zones of mineral soil. It is also shown that the links between soil physical and chemical properties and its bulk soil electrical conductivity (EC_a) measured by EMI are complex in zones of shallower peat. Additionally, this study highlights the role of pore water conductivity in influencing temporal variations in EC_a. Our findings explain the intricate interplay between peat depth, topography and EC_a in disturbed peatlands. The results of this study may be of substantial societal interest, as it provides insights into techniques for the rapid non destructive characterization of the conditions of previously drained peatlands.

1. Introduction

Peatlands provide many ecosystem services such as carbon storage, climate and water regulation, energy provision, biodiversity support, and also have cultural, recreational and educational roles (Kløve et al., 2017; Saarikoski et al., 2019). In the context of climate change, the carbon storage service is of primary importance. Peatlands are responsible for the storage of nearly 30% of the soil carbon stock globally (Minasny et al., 2023). Under natural conditions, peatlands are generally considered to be carbon sinks but with peatland degradation due to land use change or global warming they can liberate some of the stored carbon to the atmosphere (Minasny et al., 2019). This typically occurs when peat sites are drained by human intervention causing peat oxidation and release of CO_2 (Holden et al., 2004). Northern peatlands are formed in humid zones with cool temperatures and a topography allowing water retention (Jaquemart and Angenot, 2004). Peat is composed of the accumulation of partially decayed organic material and is a substrate with a high porosity, a low bulk density, a high water content, a low pH and a high organic matter content (Andersen et al., 2011; Walter et al., 2018).

Peatlands display considerable spatial and temporal heterogeneity (Walter et al., 2019; Altdorff et al., 2016), and it makes it challenging to accurately study peatland processes. This is particularly the case for the processes occurring in their subsurface (i.e., the part of the Critical Zone between the Earth surface and the bedrock below). The soil subsurface is indeed highly heterogeneous resulting from complex and multi-scale interactions between physical, biological and geochemical processes (Binley et al., 2015). These processes are of primary importance, notably to quantify the peatlands carbon stocks. Despite this, few methods allow to study them with a sufficient spatial and temporal resolution (Vereecken et al., 2016; Parsekian et al., 2015) which limits their consideration in Earth system models (Romero-Ruiz et al., 2018). Geophysics is an efficient tool in this context as it includes a series of noninvasive methods allowing to investigate the heterogeneity of the subsurface's physical properties and dynamics across larger scales (Vereecken et al., 2016; Binley et al., 2015). A range of geophysical methods exist for sensing different properties (McCann et al., 1997) and their combination allows to combine different sensitivities, resolutions and measured physical properties (Fan et al., 2020; Parsekian et al., 2015). However, several key challenges remain in geophysical investigation as: (i) process understanding requires very high spatial and temporal resolutions, (ii) the physical relationship between the properties sensed and those of interest can be uncertain, and (iii) the geographical diversity of studied sites remains limited (Binley et al., 2015; Banwart et al., 2013; Gaillardet et al., 2018).

Ground-penetrating radar (GPR) has already been used to map peat thickness, peat internal structure and soil horizons (Wastiaux and Schumaker, 2003; Walter et al., 2016; Proulx-McInnis et al., 2013; Lowry et al., 2009). The use of GPR in peat environments enables the identification of continuous and diffused reflectors indicating an interface between different hydro-pedological properties of the deposit (Wastiaux and Schumaker, 2003; Wastiaux et al., 2000). The continuous reflectors consist in contrasts in humification level, peat type, water saturation degree or different soil horizons (Wastiaux and Schumaker, 2003; Walter et al., 2016; Comas and Slater, 2004; Theimer et al., 1994; Lowry et al., 2009). The interface between peat and mineral soil is particularly easy to delineate because of the high contrast in electrical properties (Walter et al., 2016; Lowry et al., 2009). Diffused reflectors can be zones of open water, stumps or drains (Theimer et al., 1994). Most studies use GPR center frequencies of 100 to 400 MHz. The challenges remaining in the use of GPR to characterize peat subsurface are: the need to complement the measurements with in situ sampling, the transition between different horizons is not always contrasted enough to produce a radar echo and the imaging depth can be limited by high electrical conductivity (Theimer et al., 1994; Proulx-McInnis et al., 2013; Doolittle, 1987).

Electromagnetic induction (EMI) has already been used to assess peat stratigraphy (Slater and Reeve, 2002), thickness (Beucher et al., 2020; McLachlan et al., 2021) and carbon stock (Altdorff et al., 2016). Silvestri et al. (2019) showed that the electrical conductivity of peat varies a lot more than in other types of soils. Previous peatland studies showed a soil conductivity typically between 0 and 40 mS/m and usually less than 15 mS/m (Theimer et al., 1994). Peat electrical conductivity is mainly determined by the volumetric water content, the pore fluid conductivity and the surface electrical conductivity of the particles (Walter et al., 2015). There is notably a difference between bogs that are mainly fed by rainwater (characterized by low ionic concentrations) and fens that have a larger groundwater influence (high concentration of dissolved salts) and thus a higher electrical conductivity (Walter et al., 2018; Andersen et al., 2011).

The subsurface of peatlands is recognized as a crucial component controlling its ecosystem functioning, yet our understanding of its heterogeneity remains limited. Geophysical tools can be used to sense heterogeneous peatlands but their interpretation remains relatively complex. The objective of this study is to characterize and understand the heterogeneity of a peatland subsurface structure by an integrative geophysical study. The study site, located in the Belgian Hautes Fagnes, is a central-Europe disturbed peatland (previously drained for forestry), which is a poorly studied biotope. This site is also of particular natural interest in the region and of climatic interest globally. The GPR is used to characterize the peatland subsurface along a clear topographic gradient with a particular focus on the peat depth and its controlling factors. We also provide an in-depth analysis of the spatial and temporal patterns of the electrical conductivity aiming to identify the main parameters influencing this variable. Finally, we discuss the advantages and limitations of the simultaneous use of these instruments in previously drained peatlands.

2. Methods

2.1. Study site

The study site is a peatland located in the Belgian Hautes Fagnes (Fig. 1). This central-Europe disturbed peatland represents a poorly studied biotope (Walter et al., 2015). Peatland environments cover only 0.75% of the Belgian territory, the majority of which are located in the nature reserves on the *Ardennes Massif* (Frankard, 2004). The Cambrian massif consists of early Paleozoic metamorphic rocks, mostly phyllites and quartzites (Demoulin and Hallot, 2009). The present-day elevation of the Hautes Fagnes is the result of Quaternary rock uplift and the elevation of the north-eastern part of the *Ardennes Massif* increased by 700 m (Sougnez and Vanacker, 2011). The region has a cold and humid climate with 1440 mm of rain per year and a mean annual temperature of 6.7 °C (Mormal and Tricot, 2004). These peatlands were formed c. 14,000 years ago, at the end of the last glaciations (Demoulin et al., 2018). The Hautes Fagnes peatlands provide a typical fauna and flora of great ecological interest in Belgium (Wastiaux et al., 2000). During the 19*th* and 20*th* centuries, there was a reduction of the peatlands surface due to peat exploitation as well as spruce forestry. In order to preserve the peatlands from further degradation, the natural reserve of the Hautes Fagnes was created in 1957 and restoration initiatives began in 1993 (Jaquemart and Angenot, 2004; Frankard, 2004).

The study site was drained and planted with spruces in 1914 and 1918, which were cut between 2000 and 2016. Since 2017, the site is a part of the natural reserve of the Hautes Fagnes and in active restoration with selective removal of conifers. As a result, the zone is left to its natural evolution and few hardwood plantations (mainly birch and oak) more adapted to the environment were made. The study was centred on a 800 m long topographic transect (Fig. 1). This South-North oriented toposequence covers a 31 m elevation difference from the plateau position to the river valley of the *Polleur*. The slope ranges from 0 to 4° on the site with a mean slope of 2.2°. According to the soil map of Wallonia, the majority of the soil in the site is classified as peat, which is here defined as a soil with an organic matter content greater than 30% and corresponds to a histosol. In the central, southern and northeastern part of the site, the peaty topsoil overlies a silty more permeable horizon that contains fragments of schist and sandstone at its base (Bah et al., 2005).

2.2. Ground-penetrating radar

Ground-penetrating radar (GPR) sends electromagnetic waves into the soil to study its composition and structure by detecting the contrasts in the soil electromagnetic properties. The subsurface can be mapped in two or three dimensions which allows to detect the depth and the extent of subsurface horizons and of some local objects (Doolittle, 1987; Luo et al., 2019). Antennas are pulled above the surface and transmit a short duration pulse of electromagnetic energy with an ultrawide frequency band. The higher the frequency, the higher the resolution, but the lower the sensing depth (Theimer et al., 1994). The energy pulse is attenuated as it penetrates the soil depending on the electrical conductivity distribution, and a fraction of it is reflected at the electromagnetic interfaces depending on the relative dielectric permittivity contrasts. The antenna
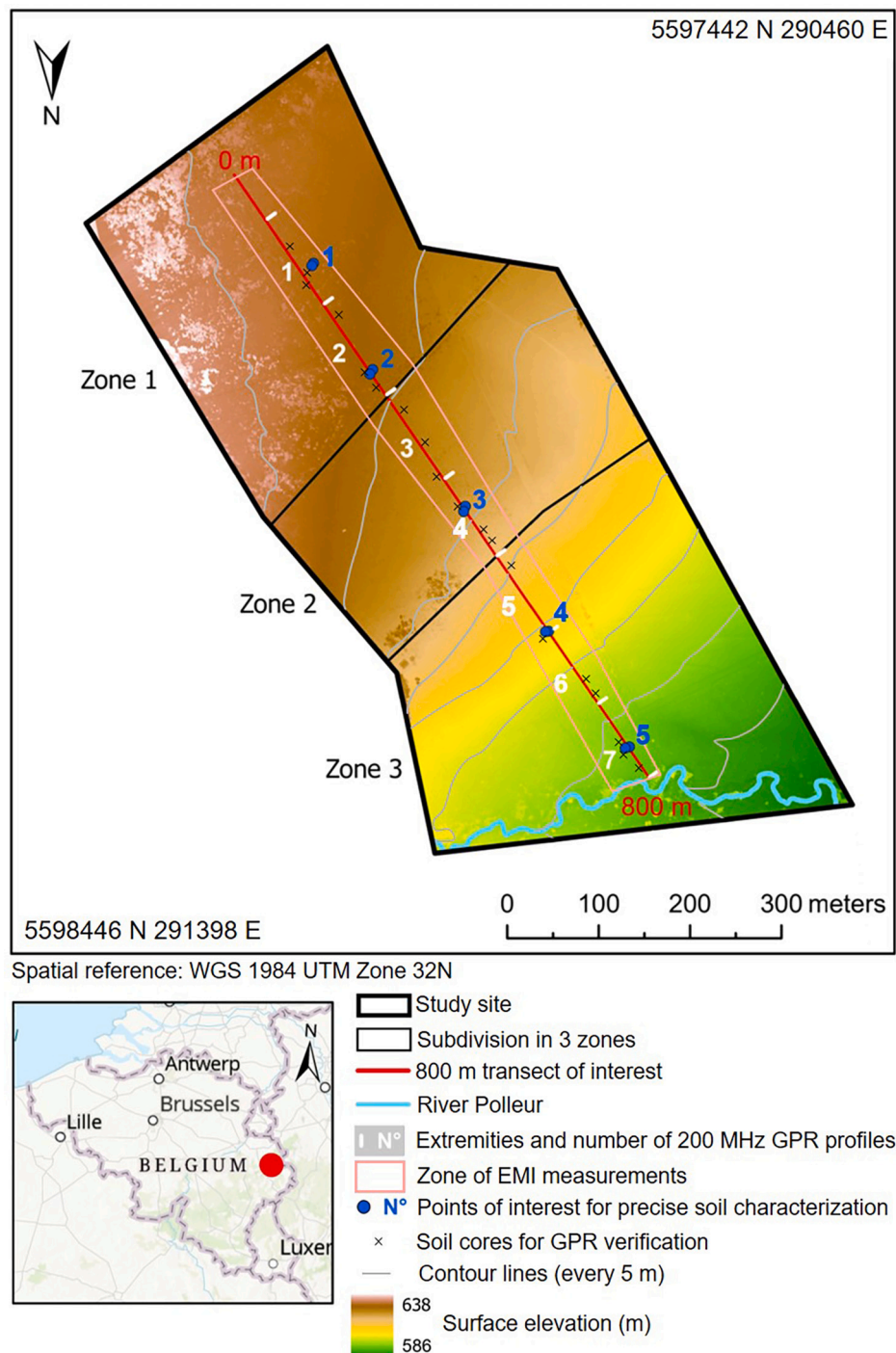
Fig. 1. Localization of the study site. The main zone is divided into three smaller zones, from South to North: zone 1 (plateau), zone 2 (plateau to gentle slope) and zone 3 (slope to river). A 800-m transect was established following the topographic gradient in order to conduct geophysical measurements. The location of the EMI measurements, the seven GPR 200 MHz profiles, the nineteen soil cores for the peat depth validation and the ten points (five groups of two) where a precise soil characterization was conducted are indicated. The surface elevation (15 cm resolution) was retrieved using a LiDAR scanner (Zenmuse L1, DJI, China).

subsequently records the returning pulse in time (Inman et al., 2002). Usually the results need to be post-processed following these steps: conversion of the time into depth, application of a gain function, average background removal and eventually the addition of some temporal and spatial frequency filters (Luo et al., 2019; Neal, 2004).

The measurements in this study were conducted with a SIR-20 GPR (Geophysical Survey Systems Inc., Nashua, New Hampshire, USA) with a 400 MHz center frequency antenna on June 1, 2022 and with a 200 MHz center frequency antenna on May 16, 2023 (Fig. 2a). The antennas were pulled above the ground by foot. The 800 m transect of interest was subdivided into about 100 m long sensing lines (Fig. 1). Along the transect, the radar data were acquired every cm. The data were processed using the Geolitix software (Geolitix Technologies INC, Canada). The relative dielectric permittivity of the peat soil was estimated to 60 based on a depth calibration using the real depth of the peat-mineral interface identified with manual augering. This value is coherent with other peatland studies (Parry et al., 2014; Theimer et al., 1994). On all images the time zero was corrected (to 9 ns for the 200 MHz antenna and

Fig. 2. Pictures of the geophysical measurements performed in this study. (a) Ground-penetrating radar measurements using the SIR-20 GPR equipped with a 200 MHz center frequency antenna (GSSI, USA). (b) Electromagnetic induction measurements using the EM38-MK2 system (Geonics, Canada).

4 ns for the 400 MHz antenna) and an average background subtraction was realized in order to highlight heterogeneities. Time range was adjusted based on the limit of GPR energy propagation and set to 120 ns, corresponding to 2.5 m depth for the 200 MHz antenna and to 55 ns, corresponding to a depth of 1.1 m, for the 400 MHz antenna.

2.3. Soil cores for GPR verification

Soil coring by hand is required to detect the nature of the interfaces identified in the GPR profiles (Sass et al., 2010). Nineteen cores were thus collected along the topographic transect to support the interpretation of the GPR images. Their location is presented on Fig. 1. Some cores were made to 1 m depth (initially to validate 400 MHz GPR measurements) and others to 2 m depth to allow a deeper soil characterization and the eventual identification of the bedrock depth. The thickness of the soil horizons was measured and the horizons were described for colour, texture, drainage and coarse fragment content. No further soil characterization was conducted on these 19 soil cores. We examined the correspondence of peat depth between GPR data and soil cores using Lin's concordance correlation coefficient. This statistic quantifies the agreement between two measurements of the same variable.

2.4. Electromagnetic induction

Electromagnetic induction (EMI) is a geophysical technique transmitting low frequency energy in the ground allowing to measure the bulk soil electrical conductivity (EC_a) (McNeill, 1980). Its unit is S/m. A transient primary magnetic field is induced by powering the transmitter coil with an alternating current in the EMI instrument. This field induces eddy currents in the soil that generates a secondary magnetic field proportional to these currents with an amplitude and phase depending on the soil electrical conductivity and magnetic susceptibility. Both the primary and secondary fields are detected by the receiver coil. However, as the primary field is known, the secondary field can be determined. Initially, electromagnetic induction was used to map soil salinity in agriculture (Doolittle and Brevik, 2014). But soil electrical conductivity is impacted by a large variety of other factors such as water content, structure, bulk density, temperature, clay content and cation exchange capacity (Abdu et al., 2007). The soil electrical conductivity is now thus

widely used to identify field-scale homogeneities and heterogeneities in order to plan soil sampling schemes or to delineate agricultural management zones (Inman et al., 2002; Stroh et al., 2001).

The measurements in this study were conducted using the EM38-MK2 (Geonics Limited, Mississauga, Ontario, Canada) operating at a frequency of 14.5 kHz (Fig. 2b). The EM38-MK2 system used has two coil spacings, i.e., 0.5 m and 1 m. However, the data from the 0.5 coil spacing were not consistent (e.g., negative values were obtained despite a proper system calibration, probably due to the small electrical conductivity encountered on the site as well as to the uneven surface conditions) and were therefore not used in this study. The instrument was thus used in vertical mode with a spacing of one meter between the coils. This allows the measurement of bulk soil apparent electrical
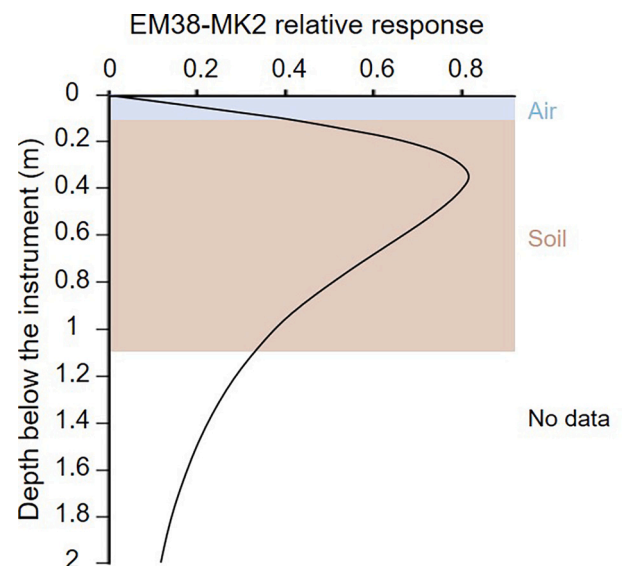

Fig. 3. Sensitivity of the EMI measurement to depth for measurements in vertical mode with a 1 m spacing between the coils (McNeill, 1980). The 0 depth corresponds to the bottom of the device. The first 10 cm sensed are the air. Then, a soil layer of 1 m is considered to analyze the link between EC_a and soil properties.

conductivity (EC_a) to 2 m depth with a maximal sensitivity at 0.4 m depth. The sensitivity of the measurement to the different depths is presented in Fig. 3. It is worth noting that the use of EMI with a single coil spacing and orientation limits the ability for depth-dependent characterization. An instrument with larger coil spacings would have been necessary for vertical conductivity profile reconstruction at this site. The instrument was warmed up for 20 min before the measurements, calibrated every two hours and protected from direct sunlight to prevent temperature influence on the measurements (Robinson et al., 2004; Abdu et al., 2007). The measurements were conducted six times at different seasons: on February 9, 2022, March 28, 2022, June 24, 2022, December 7, 2022, June 19, 2023 and September 6, 2023. The measurements were made on foot along the transect of interest (Fig. 1). The EM38-MK2 was held at a height of 10 cm above the ground. The zone measured was 800 m long and between 25 and 50 m wide. The spacing between the measurements lines was of about 10 m (2 to 4 lines were conducted depending on the dates). The inline spacing was of about 10 cm. The outliers in the data were removed (2 times the standard deviation around the mean of the EC_a distribution). The point measurements were then kriged in R (Posit, Boston, Massachusetts, USA). The grid size is 1 m and the variogram follows an exponential model with a nugget of 0.2 to 0.28 mS^2/m^2, a sill of 0.97 to 2.19 mS^2/m^2 and a range of 16.6 to 67.1 m following the different dates and instrument stability.

2.5. Soil characterization

Five locations of specific interest were selected (Fig. 1). Their position was chosen based on the topography and the variations in EC_a. At each of these points there are two replicate soil profiles located 5 m apart. The main soil horizons of these 10 points are presented in Fig. 4. Key soil chemical and physical analyses were conducted in these 10 representative soil profiles (peat depth, bulk density, saturated hydraulic conductivity, saturated water content, water content at field capacity, soil organic carbon, soil total nitrogen and texture). The time-lapse monitoring of soil physical properties (volumetric water content, soil pore water electrical conductivity and soil temperature) was performed at the same positions for the period of October 2022 to October 2023 (see below). These constant and variables properties were compared with the EC_a measurements to allow the interpretation of the EC_a spatial and temporal variations.

2.5.1. Static soil properties

In total, 30 undisturbed soil samples were collected with 100 cm^3 metal rings at three different depths in each profile: 10 cm, 30 cm and a last depth between 50 and 90 cm (Fig. 4). The lowest sample was taken in the mineral horizon below the peat when feasible (on 6 profiles out of

10). For each of these samples the bulk density was determined after drying the soil for at least 48 h at 105 °C. The saturated volumetric water content was also determined on these samples after their saturation. Then, after applying a suction of 0.1 bar with pressure plates, the volumetric water content at field capacity was measured. Finally, the saturated hydraulic conductivity was also measured with a constant head permeameter (Eijkelkamp, Netherlands). The vertical head gradient applied was of 1.8 cm.

We also collected 48 disturbed soil samples in these 10 soil profiles at depths from 0 to 100 cm. About 5 samples were collected in each profile corresponding to the variations in the soil horizons (peat or mineral soil as well as peat colour differences). These samples were dried at 80 °C for 48 h then sieved at 2 mm for soil total nitrogen (STN), soil organic carbon (SOC) and texture analysis by VIS-NIR spectroscopy modelling. For that, a specific soil spectral library for the study site was created previously by Li et al. (2024). The 48 samples of this study were then scanned in the VIS-NIR range (350–2500 nm) using a ASD FieldSpec 3 FR spectroradiometer (Analytical Spectral Devices Inc., USA) and clay and silt content, SOC and STN were estimated. These predictions are robust as prediction uncertainties are low and Root Mean Square Error (RMSE) are of 1.74 g/100 g for SOC (mineral soil), 3.84 g/100 g for SOC (peat soil), 0.05 g/100 g for STN (mineral soil), 0.19 g/100 g for STN (peat soil), 5.58 g/100 g for silt content and 1.31 g/100 g for clay content. We refer to Li et al. (2024) for more details.

2.5.2. Dynamic soil properties

In the 10 soil pits described above, 30 Teros12 sensors (Meter Group, München, Germany) were installed horizontally at three different depths: 10 cm, 30 cm and between 50 and 90 cm (i.e., the same depth at which the undisturbed soil samples were taken). These sensors measured four variables: soil volumetric water content, bulk soil electrical conductivity (referred to as $EC_{a,Teros12}$), soil pore water electrical conductivity (σ_w) and soil temperature at a time step of 10 min starting from October 2022. Teros12 sensors are using an electromagnetic field to measure the dielectric permittivity of the soil, which is then converted into volumetric water content after a soil specific calibration. This calibration was realized by rewetting various soil samples from the study site, following the manufacturer recommendations. The temperature is measured with a thermistor located in the sensor central needle. Teros12 applies an alternating current to two electrodes and measures the resistance between them, which allows to measure the soil electrical conductivity. This conductivity can then be converted into pore water electrical conductivity using an equation derived from Hilhorst (2000). To investigate the influence of soil water content, soil pore water electrical conductivity and soil temperature on EC_a dynamics, a dataset of 30 measurements was used: the 10 profiles of interest at three dates of
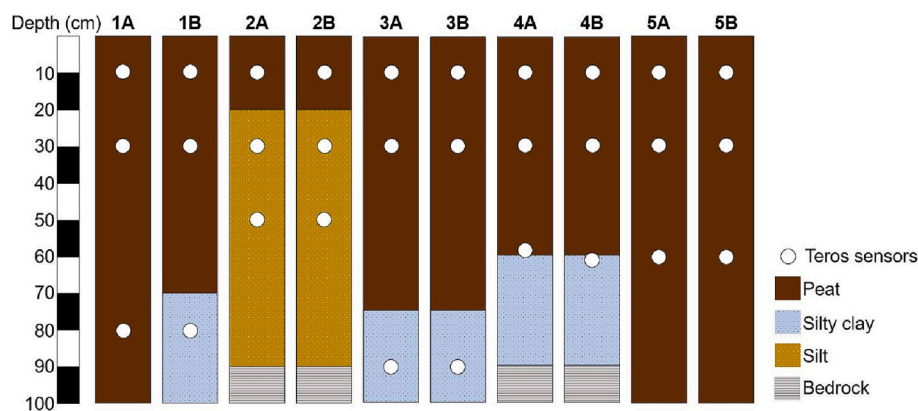

Fig. 4. In the 10 soil profiles, the soil hydrophysical and geochemical properties were determined. The profiles are located at 5 topographic positions, as presented in Fig. 1, each with two different profiles distant of 5 m labelled as A and B. This figure presents the pedological interpretation to a depth of 1 m of these 10 profiles. The location of the Teros12 sensors also corresponds to the location where undisturbed soil samples were collected.

contrasting hydrological conditions (December 2022, June 2023 and September 2023). The daily average of the variables of interest was considered here.

2.5.3. Integration of soil properties with EMI

The EM38-MK2 measures EC_a at each location, providing an integrated reading of the EC_a down to a depth of 2 m, with the relative response varying according to depth (Fig. 2). All the previously mentioned static and dynamic soil properties should thus be integrated on the whole profile to provide a single value that can be comparable with the EM38-MK2 results. The first 10 cm sensed were considered as air. Then, the soil properties of the first meter of the 10 soil profiles of interest were considered (no data were available deeper). This first meter still represents 79% of the EM38-MK2 relative response and is

thus already a relatively good representation. First, all the measured variables (at 3 to 5 depths depending on the considered variable) were linearly interpolated every 10 cm in the profile and depending on the different soil layers to acquire a continuous characterization. Then, the values of the variables at each depth were weighted according to the EMI relative response (Fig. 2). The EC_a at each of the 10 points is determined as the average EC_a within a 1.5 m diameter around these points (Callegary et al., 2012).

The link between this soil characterization and the EC_a was analyzed using R (Posit, Boston, Massachusetts, USA). First, Spearman correlation (Rs) values are presented. To evaluate the relationship between two variables while isolating the effect of another correlated variable, partial correlation analyses were also performed (using the *ppcor* package).
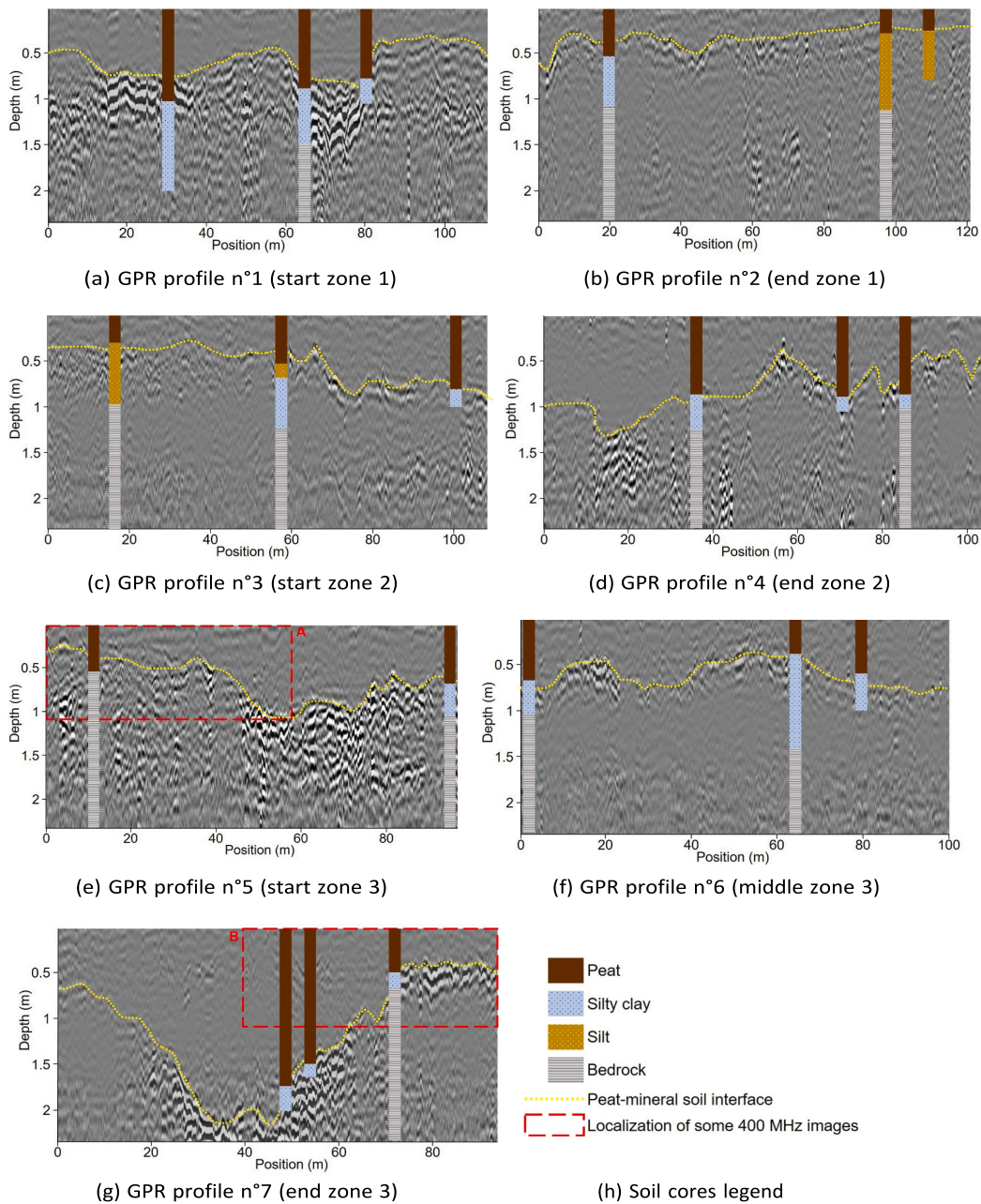

(a) GPR profile n°1 (start zone 1)

(b) GPR profile n°2 (end zone 1)

(c) GPR profile n°3 (start zone 2)

(d) GPR profile n°4 (end zone 2)

(e) GPR profile n°5 (start zone 3)

(f) GPR profile n°6 (middle zone 3)

(g) GPR profile n°7 (end zone 3)

(h) Soil cores legend

Fig. 5. The seven GPR profiles realized along the transect with the 200 MHz antenna (location presented in Fig. 1). The horizontal axis corresponds to the position along the profile (the 0 is always uphill). The vertical axis presents the soil depth. The grey colour scale is the normalized amplitude of wave reflection. The yellow line underlines the interface between peat and the underlying mineral soil and was visually identified based on the amplitude of wave reflections. The 19 soil cores conducted are schematized with their different soil horizons and are presented at the correct location.

3. Results and discussion

3.1. Ground-penetrating radar imaging

3.1.1. GPR and soil cores results

Fig. 5 presents the seven GPR profiles realized along the transect with the 200 MHz antenna. This figure presents the amplitude of the GPR wave reflections as a function of depth and distance along the profile. The most important reflections are interpreted as interfaces between soil horizons of different electromagnetic properties. The first major reflection represents the interface between peat and the underlying mineral soil. It can easily be identified because there is a high difference in water content between those two layers resulting in a high dielectric permittivity contrast that will reflect the electromagnetic waves (Zajıcova and Chuman, 2019). This interface was visually identified thanks to its clarity. Nevertheless, implementing a change detection algorithm would be advised when dealing with a larger amount of data. As the focus of the current study is on peat characterization, eventual deeper reflectors are not discussed in detail. Along the toposequence, the peat depth is ranging from 0.2 to 2.1 m, with a depth of 0.5 to 1 m on most of the studied transect.

Nineteen soil cores of 1 to 2 m depth were taken along the transect. They are schematized in Fig. 5 and aligned to the GPR profiles. The comparison between the subsurface images conducted with the GPR and the soil cores allow us to interpret the different horizons present in the soil subsurface. Most of the profiles show a peat horizon, followed by a compact silty clay horizon and by the bedrock. Regarding the peat depth, there is a good correspondence between the information derived from the soil cores measurements and the data extracted from GPR images (Fig. 6). The maximum difference is c. 20 cm and the RMSE is 11 cm based on the comparison of the 19 points. The Lin's concordance correlation coefficient is 0.96. The slight discrepancies could be a result of the limited precision of the GPR's GPS with respect to the local soil variability, the estimation of the wave velocity, the microtopography, the uncertainty on the time zero and the uncertainty on the delineation of the top of the reflections on the GPR images.

The 400 MHz images are shallower (about 1 m) and thus mainly characterize the peat. They show fewer significant reflections than the 200 MHz images. Two images showing more reflection than the others are presented in Fig. 7 and their corresponding localization with the 200 MHz images are presented in Fig. 5e and g. These two images show a weak reflection corresponding to the peat-mineral interface between depths of 0.3 and 1 m. They show quite similar reflections as on the corresponding 200 MHz ones but are less clear. Wastiaux and Schumaker (2003) and Theimer et al. (1994) were able to identify the interface between the acrotelm and catotelm (two distincts layers in peat bogs containing living plant or dead plant material, respectively) in their
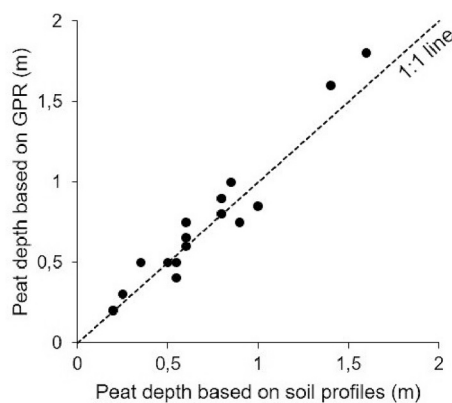

Fig. 6. Scatterplot of the peat depth based on 200 MHz GPR imaging and the 19 manual soil cores collected. The 1:1 line is presented on the graph. The RMSE is 11 cm and the Lin's concordance correlation coefficient is 0.96.

studies but this is not visible here. The water table was estimated to be located around 30 cm depth on the day of measurement and was maybe too shallow to be separated from the surface reflection. Furthermore, the identification of water table depth with GPR is complicated in fine-grain soils due to the capillary fringe (Pathirana et al., 2023). Previous studies also identified differences in peat humification stage based on GPR images (Kettridge et al., 2008; Walter et al., 2016; Wastiaux and Schumaker, 2003), but this was not visible in our study.

3.1.2. Soil horizon depth variations along the toposequence

Fig. 8 presents a summary diagram illustrating the peat depth along the toposequence. This image shows the potential of GPR to capture complex variations in peat depth. The peat depth substantially varies at small scales but mainly varies between 0.5 and 1 m. The observed peat depths in our study are consistent with other studies conducted in the same region (Wastiaux and Schumaker, 2003). The soil layer situated below this peat is a gleyed layer rich in clay, which originates from the alteration of the underlying parent material. This silty clay layer is relatively impermeable which favoured water stagnation and the development of peat soils (Wastiaux and Schumaker, 2003). A zone with a shallow organic horizon, about 20 cm depth, followed by a horizon rich in silt and rock fragments, was found at the end of zone 1 and the beginning of zone 2 (Fig. 5b and c). This is consistent with the soil map of Wallonia (Bah et al., 2005) showing a zone of silty soil with moderate to poor drainage at the same location. The GPR allows to delineate more clearly the extent of this silt lens: from 85 m in Fig. 5b to 60 m in Fig. 5c. The thickest organic horizons (with a depth of more than 2 m) were found at the bottom of the hillslope (Fig. 5g). However, in the last 30 m of zone 3, near the river, the peat is only 0.5 m deep (Fig. 5g). The decrease in peat depth at the footslope is attributed to the presence of Quaternary deposits in the river valley of the *Polleur* river (Demoulin et al., 2018).

#### 3.1.3. Topographical control on peat depth

First, peat depth shows a significant Spearman correlation with elevation (-0.43, p-value of 4.10^{-8}). Peat depth also shows a significant Spearman correlation with the topographic wetness index (0.24, p-value of 0.003). This index is commonly used to quantify topographic control on hydrological processes, calculated as $\ln(\alpha/\tan(\beta))$ where α is the upslope area draining to one point and β is the slope (Beven and Kirkby, 1979). On the contrary, peat depth shows no significant correlation with slope. This shows that a part of the observed variability in peat depth can be related to topography, especially in the bottom of the toposequence where the peat is deeper. This can be explained by the fact that this zone is a zone of accumulation of water which favours peat development. However, it should be noted that in the last 30 m of the transect this is not applicable due to the occurrence of the Quaternary deposits. In contrast to other studies that have reported thinner peat on slopes of similar magnitude (Poggio et al., 2020; Wastiaux and Schumaker, 2003) we found no direct effect of the slope on the peat depth. We can thus conclude that on this site, which is characterized by a heterogeneous peat depth, topography explains only a part of the observed variability. We argue that the recent land use history is unlikely to be a major influence on peat depth since the three zones were planted with spruce from 1914 or 1918 to 2008 (zone 1), 2012 (zone 3) and 2016 (zone 2). The presence of the silt lens is reducing the peat thickness, as it favours a higher water infiltration capacity. Other controls that could further explain peat depth variability include micro topography and spatial variability in bedrock composition and permeability along and across slope. However, both controls are not included in the larger scale trends of elevation and topographic wetness index that we used in our analysis.

3.2. Soil electrical conductivity

3.2.1. Electrical conductivity measurements

The EC_a was measured using EMI on six different dates between

(a) GPR profile A (start zone 3)   (b) GPR profile B (end zone 3)
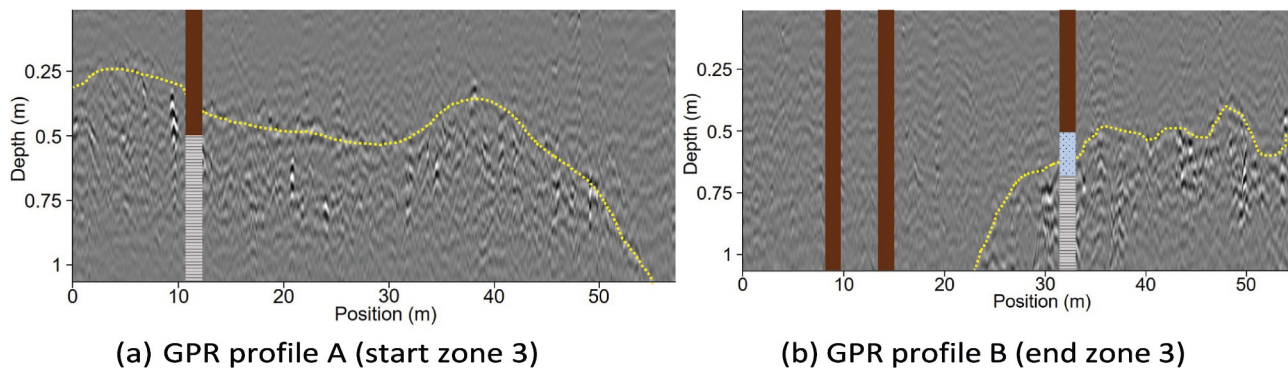
Fig. 7. Two of the ten profiles realized along the transect with the 400 MHz antenna. Their location relatively to the 200 MHz profiles are presented in Fig. 5. The horizontal axis is the position along the profile and the vertical axis is the soil depth. The grey colour scale is the normalized amplitude of wave reflection. The yellow line underlines the interface between peat and the underlying mineral soil.
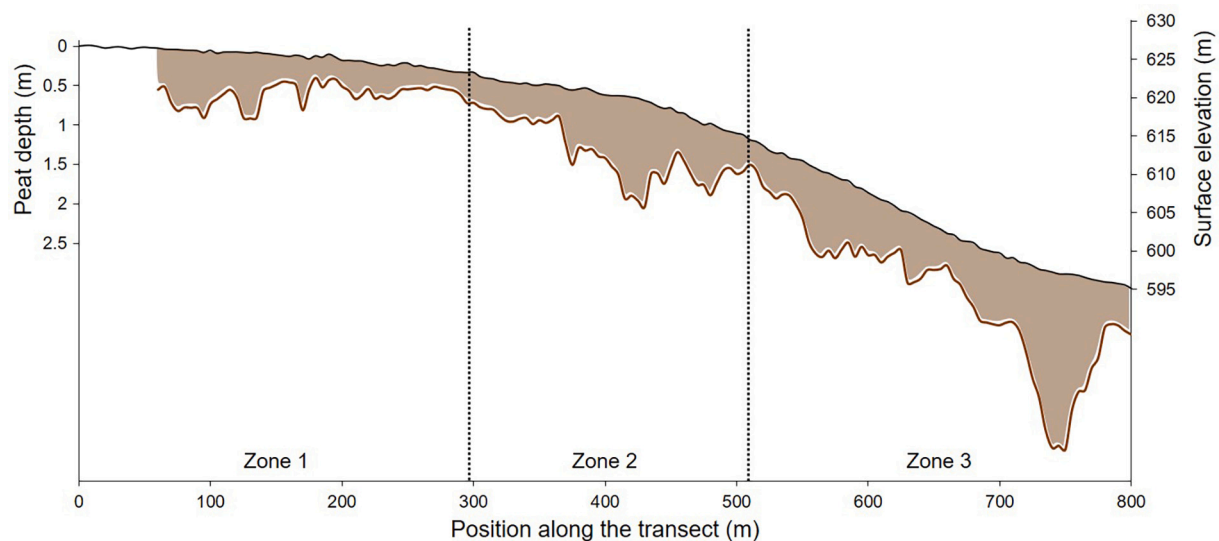
Fig. 8. Summary diagram of peat depth along the profile derived from the GPR images. The peat depth scale is 10 times larger than the surface elevation scale.

February 2022 and June 2023. The observed EC_a values ranged between 5 and 17 mS/m while the mean EC_a of each measurement date ranged between 9.8 and 11.7 mS/m and had a standard deviation of c. 1.5 mS/m. This is consistent with the study of Theimer et al. (1994) who reported that most of the EC_a observations in peatlands are below 40 mS/m and often less than 15 mS/m. Working in the same region as this study, Wastiaux and Schumaker (2003) found EC_a values mainly below 10 mS/m. This also suggests that this site would be a bog, meaning that it is fed by rainwater which leads to low conductivities (Doolittle and Butnor, 2009). It is worth noting that these relatively low EC_a values are highly advantageous for GPR imaging, despite the high water saturation level.

Fig. 9 presents the temporal evolution of the EC_a along the transect. During the observation period, a zone of higher EC_a is identified in the middle of zone 1. In February and March 2022, zone 2 exhibited a lower EC_a compared to the rest of the site, but it was higher on the other dates. The discontinuity between zone 2 and zone 3 in February and March 2022 can be explained by the presence of a 1-m-high artificial embankment around zone 2 creating a capillary barrier preventing the water flow. Zone 3 is showing a relatively homogeneous EC_a across space and time.

3.2.2. Impact of static soil properties on spatial variability of electrical conductivity

The EC_a can be related to other variables to facilitate the interpretation of the EC_a patterns observed at the site and determine if it could be used as a proxy for other soil properties. A detailed comparison between EC_a and static soil properties (peat depth, bulk density, saturated hydraulic conductivity, saturated water content, water content at field capacity, SOC, STN, silt content, clay content) was conducted for 10 validation points. These static properties were weighted in function of depth according to the EMI relative response. For these 10 points, the EC_a of the six different dates was temporally aggregated and ranges from 9.5 to 14.0 mS/m. The Spearman correlations (Rs) between the EC_a and these factors are presented in Table 1. The Spearman partial correlations, with peat depth as an explaining factor, are also presented. This allows to study the correlation between EC_a and soil properties without any influence from the peat depth which influences greatly the other parameters.

On one hand, bulk density shows a relatively low negative correlation with EC_a (− 0.33), while the partial correlation is higher when taking peat depth into account (−0.57). On another hand, SOC and STN are positively and significantly correlated to EC_a (respectively with a partial Rs of 0.63 and 0.66). This contradicts other studies associating humification with EC_a and showing an increase in EC_a when bulk density increases and carbon content decreases in peat (Ekwue and Bartholomew, 2011; Walter et al., 2015; Asadi and Huat, 2009). In this study, EC_a is negatively correlated with bulk density and positively correlated with SOC. This suggests that peat humification may be negatively correlated with EC_a. As peat decomposition varies
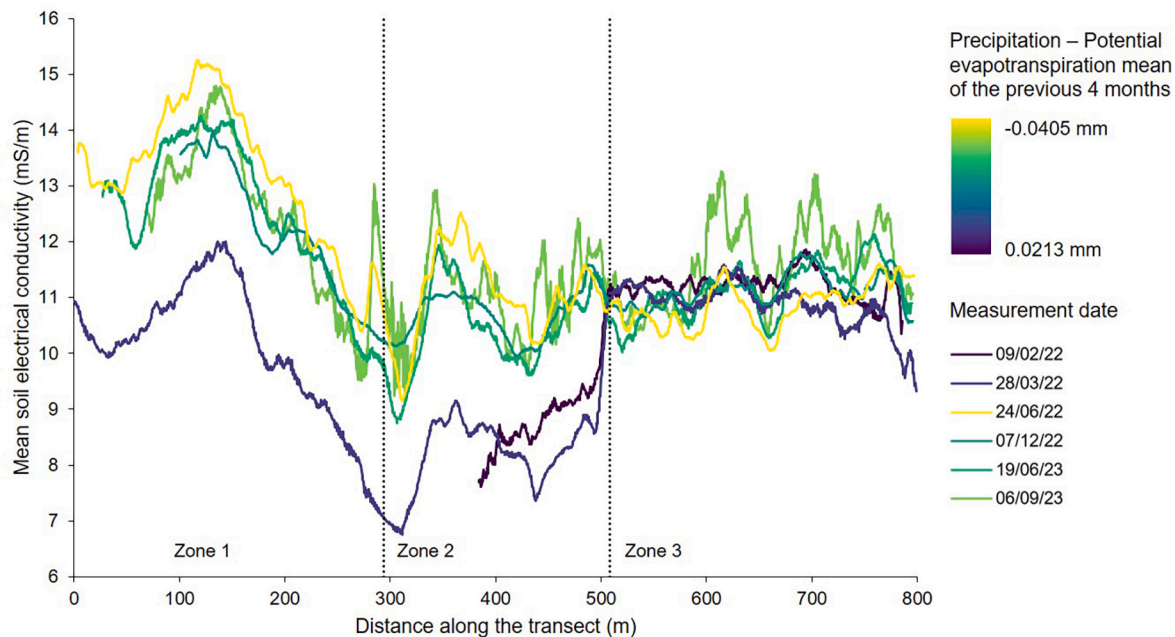
Fig. 9. Mean of the EMI-derived EC_a (on the different acquisition lines) along the 800-m toposequence (from the top to the bottom of the slope) for the six dates of measurements. The colour scale indicates the mean amount of precipitation minus potential evapotranspiration during the four months preceding the measurement date.

Table 1

First order and partial correlation of temporally aggregated EC_a (on the six sensed dates) with the static soil properties. For the Spearman partial correlation, the peat depth is the controlling factor since it affects greatly all the other parameters.* Means the *p*-value is below 0.1.

	Spearman correlation	Spearman partial correlation
Peat depth (cm)	0.20	
Bulk density (g/cm³)	-0.33	-0.57
Saturated hydraulic conductivity (log m/s)	0.58 *	0.56
Saturated water content (cm³/cm³)	0.32	0.52
Water content at field capacity (cm³/cm³)	0.18	-0.04
Soil organic carbon (% weight)	0.45	0.63 *
Soil total nitrogen (% weight)	0.47	0.66 *
Silt content (% weight)	-0.47	-0.66 *
Clay content (% weight)	-0.37	-0.51

substantially at small scales (Morishita and Kawahigashi, 2018), this relation remains difficult to interpret. However, the 400 MHz GPR images showed a relatively homogeneous peat. This could mean that the peat decomposition stage is high (estimated between a humification degree of H6 to H10 according to Von Post scale) and shows little variation. However, a more likely explanation is that the mineral soil influences the EC_a since EMI integrates the EC_a over a depth of 2 m and that a part of these 2 m is mineral soil. This underlying mineral soil has indeed a high bulk density and a low EC_a on this site (between 2.5 and 14.0 mS/m depending on the position, with a mean of 7.4 mS/m according to Teros12 sensors). These results suggest that EC_a cannot be used as a proxy for peat humification stage when it is measured with the EM38-MK2 (or a similar instrument) with a single coil spacing and orientation on peats shallower than 2 m, at least in this study site. This further supports the observation made by Walter et al. (2015), suggesting that the relationship between EC_a and peat decomposition may

not be well-established. The successful use of a multi-coil/multi-frequency EMI would provide depth-dependent information (Beucher et al., 2020; Blanchy et al., 2024; McLachlan et al., 2021) and could allow to differentiate the peat and the mineral soil influence on the EC_a. This methodology would thus be advised to determine the potential of using EC_a as a proxy for peat humification state.

The saturated hydraulic conductivity shows a relatively high and significant correlation with EC_a (Rs of 0.58, and partial Rs of 0.56). These two parameters are typically correlated because electrical current flow and fluid flow in soils are analogous processes influenced by similar parameters such as porosity, connectivity and tortuosity (Doussan and Ruy, 2009). Since this site has a low clay content, the pore volume dominates the electrical flow and a positive correlation between EC_a and hydraulic conductivity is expected (Purvance and Andricevic, 2000). Saturated water content is also positively correlated with EC_a (partial Rs of 0.52). This means that higher porosity will lead to higher EC_a, as

demonstrated by Archie's law (Archie, 1942); this is particularly true when the soil profile is saturated. On the contrary, water content at field capacity shows a weak correlation with EC_a. Both saturated hydraulic conductivity and saturated water content provide information on the pore size distribution of the soil, highlighting its significant influence on soil EC_a.

The silt and clay content are negatively correlated with EC_a (partial Rs of −0.66 and − 0.51 respectively). This is quite surprising because an increase in clay content is expected to raise the EC_a (Doolittle and Brevik, 2014; Moghadas et al., 2016). This implies that the mineral soil on this site has a very low EC_a, lower than the peat.

3.2.3. Impact of dynamic soil properties on temporal variability of electrical conductivity

Earlier studies showed that peat EC_a is mainly depending on soil water content, soil pore water conductivity and electrical conductivity of the organic matrix (Comas et al., 2004; Ponziani et al., 2012a). Dynamic soil properties will thus influence EC_a dynamics. In particular, the influence of soil water content, soil pore water electrical conductivity (σ_w) and soil temperature measured by the Teros12 sensors are investigated in this study. First order and partial correlation are presented in Table 2.

Volumetric water content is slightly but not significantly correlated with EC_a (Rs of 0.12); this is logical, as an increase in water typically causes an increase in EC_a (Abdu et al., 2007). This correlation decreases when the pore conductivity is taken into account (−0.02) and increases when the soil temperature is taken into account (0.15). Comas et al. (2004) showed a positive correlation between water content and EC_a in saturated peat and Walter et al. (2019) showed the same in unsaturated peatlands (this relation being more sensitive at a high water saturation level). However, Walter et al. (2016) and Ponziani et al. (2012b) also showed that EC_a can decrease in peat when the water content increases. There is thus no scientific consensus on the influence of water content on peat EC_a and this study further highlights this variable relationship.

Soil temperature shows a non significant positive correlation (0.28) with EC_a and increases when water content or σ_w is taken into account. This is logical since an increase in soil temperature is expected to increase EC_a (Abdu et al., 2007). Nevertheless, the correlation remains small, indicating that soil temperature cannot be considered as the primary controlling factor for EC_a.

Soil pore water electrical conductivity (σ_w), which is linearly correlated to the concentration of dissolved ions (Theimer et al., 1994), has an important and significant correlation with peat EC_a (0.70). This correlation remains high and significant when taking water content and soil temperature into account. Kettridge et al. (2008) and Theimer et al. (1994) showed that σ_w can explain the spatial variation in EC_a in peatlands because of the high water content and the lack of other controlling mechanisms. Other studies also showed that the relationship between EC_a and σ_w in peatlands is non linear at low σ_w (Comas and Slater, 2004; Ponziani et al., 2012b; Walter et al., 2018). This study shows that soil pore water has a more significant influence on EC_a than water content

and soil temperature. The EMI might thus be useful to assess the ion dynamics which in turn shows correlation with dissolved organic carbon concentrations (Frank et al., 2017).

Soil bulk electrical conductivity measured by the Teros12 sensors ($EC_{a,Teros12}$) is not presented in Table 2 as it is not an explicative factor for EC_a but another way to measure the same variable. However, it is worth noting that the Spearman correlation between EC_a measured by the EM38-MK2 and $EC_{a,Teros12}$ is 0.68 and is significant. The difference between both could be due to the different sensing depths and to the difference in the volume of measurements linked with the EC_a spatial variability.

Fig. 9 shows the temporal evolution of soil bulk electrical conductivity by presenting the mean EC_a of the several EMI aquisition lines along the 800 m toposequence for six dates. In zone 1 and zone 2, the EC_a pattern is similar but there is a slight shift in EC_a amplitude as a function of the date. This shift is a small EC_a variation that might be due to some operational differences between the survey periods (such as height of the instrument, operator that conducted the calibration and air temperature). However, we hypothesized that the surveys were consistent and try to interpret this shift with regard to the environmental conditions. This shift could then be explained by the seasonal variations in precipitation and temperature that are driving soil moisture and mainly pore water conductivity changes (Inman et al., 2002; Walter et al., 2018). Thus, a higher EC_a in June and September for zones 1 and 2 can be explained by the fact that the higher temperatures increased the evapotranspiration which induced a capillary rise of soil solutes to the topsoil. Therefore, the σ_w is subsequently increased. The low EC_a in February and March is due to the fact that, along with the low temperatures, there was a lot of rain during winter which resulted in dilution of σ_w due to lateral or vertical transport of soil solutes along slope. As opposed to zones 1 and 2, the EC_a is relatively constant in zone 3, although some spatial variations can be observed. This suggests that operational influence is relatively small. This lower dynamic can be explained by the more constant hydrological conditions of this zone. Indeed, the zone is less wet in winter than the two others because of the high drainage density while it is comparatively more wet in the spring because water from uphill is flowing to this zone.

The Pearson correlation between the mean EC_a and the mean of the precipitation minus the potential evapotranspiration amount for the four months preceding the date of measurement is −0.96 and is significant (*p*-value of 0.0027). When taking the air temperature into account, the partial correlation equals −0.95 with a *p*-value of 0.011. This shows that the temperature alone is not driving these EC_a patterns, but does so in combination with seasonal variations in σ_w driven by the variations in precipitation and evapotranspiration. This observation is coherent with the study of Walter et al. (2018) who observed a higher salinity in summer and a leaching of soil solutes in spring and autumn.

Table 2

First order and partial correlation between EC_a and the dynamic soil properties measured by the Teros12 sensors. **Means the *p*-value is below 0.01.

	Spearman correlation	Spearman partial correlation (VWC as control)	Spearman partial correlation (σ_w as control)	Spearman partial correlation (soil t° as control)
Volumetric water content (cm^3/cm^3)	0.12		-0.02	0.15
Soil pore water electrical conductivity (mS/m)	0.70 **	0.70 **		0.78 **
Soil temperature (°C)	0.28	0.30	0.54 **	

Rs
1
- 0
-1

3.3. Comparing EMI and GPR approaches: advantages, limitations and complementarities

The combined use of GPR and EMI provided complementary information that is useful to gain insights into peatlands subsurface. While GPR (especially at 200 MHz) proved consistent results for quantifying the spatial variability of peat depths at a high resolution, the use of EMI sensor assisted in analyzing the temporal dynamics of EC_a which allowed for a better understanding of the underlying hydrological processes.

First, the joint use of GPR and EMI allows to study the correlation between the peat thickness and the soil bulk electrical conductivity. Earlier studies showed, when the mineral soil beneath the peat is sand, that the EC_a increases when the peat depth increases both in bogs (Altdorff et al., 2016) and in fens (Beucher et al., 2020). It is less clear however when the underlying material is clay-rich (Slater and Reeve, 2002). In this study site, there was no significant correlation between EC_a and peat depth. To test this further, the data was split into two groups (peat shallower than 1 m and thicker than 1 m) and a Wilcoxon test was conducted. This test showed no significant difference between these two groups (*p*-value of 0.88). We thus infer that EC_a is not a good proxy for peat depth on this study site. This shows that the success of EMI to determine peat depth can vary in function of studied sites. However, it should be noted that the use of single coil EMI data in this study is a major limitation. The use of multi-coil/multi-frequency EMI provides depth-dependent information and can thus be more successful to infer peat depth from EC_a measurements, particularly with a larger coil spacing than 1 m (Beucher et al., 2020; Blanchy et al., 2024; McLachlan et al., 2021).

In addition to the subsurface horizon thicknesses, the subsurface composition identified with the soil cores can be compared with the EC_a patterns. A zone of silty soil was identified by the GPR and was confirmed by the soil cores. The median EC_a for the silty zone is 9.84 mS/m while it is 11.12 mS/m for the rest of the site. The difference between these two groups is significant (*p*-value of 6.5 10^{-9} for the Wilcoxon test). Wende and Kirsch (1993) also showed a higher EC_a in peat soils than in mineral soils. This result demonstrates the potential use of EC_a to detect the lateral extensions of the peat body and the mineral soil.

Comparing the first-order Spearman correlation with the partial correlation considering peat depth as the explanatory factor (Table 1) can inform us on the importance of a priori information on peat depth when relating EC_a to static soil properties. The median difference between both correlation is 19%. It shows that the peat depth knowledge can improve the prediction of some specific soil properties using the EC_a, such as SOC and bulk density, that are essential for carbon stock estimation. Given that peat depth can be identified by GPR, the combined use of GPR and EMI has thus the potential to provide additional information when interpreting EC_a.

4. Conclusion

In this study, we characterized the heterogeneity of a disturbed peatland subsurface (above the bedrock) along a topographic gradient using geophysical instruments. The GPR was used to measure peat depth at high resolution. The peat depth ranges from 0.2 to 2.1 m and is characterized by high spatial variability. For these peat depths the use of the 200 MHz antenna yielded better results than the 400 MHz antenna. Topography could explain a part of the observed variability in peat depth.

The EMI was used to measure EC_a along a toposequence on different dates with contrasting meteorological conditions over the seasons. First, the spatial variations in EC_a were studied. Our results showed that, on this site characterized by shallow peats, the mineral soil influences the EC_a measurements. Therefore, using EC_a as a proxy for peat humification stage or soil texture is not straightforward, despite the critical

importance of accurately predicting these properties to estimate carbon stocks and plan effective restoration strategies. We also showed that the relation between EC_a and soil properties is improved when the peat depth is known, thanks to GPR measurements. We emphasize the importance of conducting further studies on the drivers of electrical conductivity in disturbed peatlands, particularly incorporating as many confounding factors as this study did, but with a greater number of point measurements. Though EMI used with a single coil spacing and orientation is not the best configuration to determine peat properties on similar sites, it can be used to delineate areas where mineral soils are present. Second, the temporal variations in EC_a were studied. This study highlights that the pore water electrical conductivity influences more the seasonality of EC_a than its water content. The EMI might thus be useful to assess the soil solutes dynamics which has an impact on the dissolved organic carbon fluxes.

This research enhances our understanding of the subsurface structure of disturbed peatlands, including the complex relationship between peat depth, topography and electrical conductivity and the main drivers of its spatial and temporal variations. It also provides valuable insights into the use of geophysical instruments to assess and manage the state of disturbed peatlands that are ecologically important and climate-sensitive ecosystems.

CRediT authorship contribution statement

Maud Henrion: Writing – original draft, Visualization, Investigation, Formal analysis, Conceptualization. **Yanfei Li:** Writing – review & editing, Investigation. **Triven Koganti:** Writing – review & editing. **Michel Bechtold:** Writing – review & editing. **François Jonard:** Writing – review & editing, Funding acquisition, Conceptualization. **Sophie Opfergelt:** Writing – review & editing, Funding acquisition, Conceptualization. **Veerle Vanacker:** Writing – review & editing, Funding acquisition, Conceptualization. **Kristof Van Oost:** Writing – review & editing, Funding acquisition, Conceptualization. **Sébastien Lambot:** Writing – review & editing, Investigation, Funding acquisition, Conceptualization.

Declaration of competing interest

The authors declare that they have no known competing financial interests or personal relationships that could have appeared to influence the work reported in this paper.

Data availability

Data will be made available on request.

References

Abdu, H., Robinson, D.A., Jones, S.B., 2007. Comparing bulk soil electrical conductivity determination using the DUALEM-1S and EM38-DD electromagnetic induction instruments. Soil Sci. Soc. Am. J. 71, 189–196. https://doi.org/10.2136/sssaj2005.0394.

Altdorff, D., Bechtold, M., van der Kruk, J., Vereecken, H., Huisman, J., 2016. Mapping peat layer properties with multi-coil offset electromagnetic induction and laser scanning elevation data. Geoderma 261, 178–189. https://doi.org/10.1016/j.geoderma.2015.07.015.

Andersen, R., Rochefort, L., Landry, J., 2011. La chimie des tourbières du Québec: une synthèse de 30 années de données. Le naturaliste canadien 135, 5–14.

Archie, G., 1942. The electrical resistivity log as an aid in determining some reservoir characteristics. Trans. AIME 146, 54–62. https://doi.org/10.2118/942054-G.

Asadi, A., Huat, B.B.K., 2009. Electrical Resistivity of Tropical Peat. Electron. J. Geotech, Eng, p. 14.

Bah, B., Veron, P., Bracke, C., Lejeune, P., Rondeux, J., Mokadem, A., Bock, L., 2005. The Digital Soil Map of Wallonia (DSMW/CNSW), Coruna, Spain.

Banwart, S.A., Chorover, J., Gaillardet, J., Sparks, D., White, T., Anderson, S., Aufdendkampe, A., Bernasconi, S., Brantley, S.L., Chadwick, O., Dietrich, W., Duffy, C., Goldhaber, M.B., Lehnert, K., Nikolaidis, N.P., Ragnarsdottir, K.V., 2013. Sustaining Earth's Critical Zone Basic Science and Interdisciplinary Solutions for Global Challenges. University of Sheffield, United Kingdom.

Beucher, A., Koganti, T., Iversen, B.V., Greve, M.H., 2020. Mapping of peat thickness using a multi-receiver electromagnetic induction instrument. Remote Sens. 12, 2458. https://doi.org/10.3390/rs12152458.

Beven, K.J., Kirkby, M.J., 1979. A physically based, variable contributing area model of basin hydrology/un modèle à base physique de zone d'appel variable de l'hydrologie du bassin versant. Hydrol. Sci. Bull. 24, 43–69. https://doi.org/10.1080/02626667909491834.

Binley, A., Hubbard, S.S., Huisman, J.A., Revil, A., Robinson, D.A., Singha, K., Slater, L.D., 2015. The emergence of hydrogeophysics for improved understanding of subsurface processes over multiple scales. Water Resour. Res. 51, 3837–3866. https://doi.org/10.1002/2015WR017016.

Blanchy, G., McLachlan, P., Mary, B., Censini, M., Boaga, J., Cassiani, G., 2024. Comparison of multi-coil and multi-frequency frequency domain electromagnetic induction instruments. Front. Soil Sci. 4 https://doi.org/10.3389/fsoil.2024.1239497, 1239497. URL: https://www.frontiersin.org/articles/10.3389/fsoil.2024.1239497/full.

Callegary, J.B., Ferré, T.P.A., Groom, R.W., 2012. Three-dimensional sensitivity distribution and sample volume of low-induction-number electromagnetic-induction instruments. Soil Sci. Soc. Am. J. 76, 85–91. https://doi.org/10.2136/sssaj2011.0003.

Comas, X., Slater, L., 2004. Low-frequency electrical properties of peat. Water Resour. Res. 40 https://doi.org/10.1029/2004WR003534.

Comas, X., Slater, L., Reeve, A., 2004. Geophysical evidence for peat basin morphology and stratigraphic controls on vegetation observed in a Northern Peatland. J. Hydrol. 295, 173–184. https://doi.org/10.1016/j.jhydrol.2004.03.008.

Demoulin, A., Hallot, E., 2009. Shape and amount of the quaternary uplift of the western Rhenish shield and the Ardennes (western Europe). Tectonophysics 474, 696–708. https://doi.org/10.1016/j.tecto.2009.05.015.

Demoulin, A., Juvigné, E., Houbrechts, G., 2018. The periglacial ramparted depressions of the Hautes Fagnes plateau: Traces of late Weichselian lithalsas. In: Landscapes and Landforms of Belgium and Luxembourg. Springer, pp. 101–113.

Doolittle, J.A., 1987. Using ground-penetrating radar to increase the quality and efficiency of soil surveys. In: Soil Survey Techniques. Soil Sci. Soc. Am. J., pp. 11–32.

Doolittle, J.A., Brevik, E.C., 2014. The use of electromagnetic induction techniques in soils studies. Geoderma 223-225, 33–45. https://doi.org/10.1016/j.geoderma.2014.01.027.

Doolittle, J.A., Butnor, J.R., 2009. Soils, peatlands, and biomonitoring. In: Ground Penetrating Radar Theory and Applications. Elsevier, pp. 177–202.

Doussan, C., Ruy, S., 2009. Prediction of unsaturated soil hydraulic conductivity with electrical conductivity. Water Resour. Res. 45 https://doi.org/10.1029/2008WR007309.

Ekwue, E., Bartholomew, J., 2011. Electrical conductivity of some soils in Trinidad as affected by density, water and peat content. Biosyst. Eng. 108, 95–103. https://doi.org/10.1016/j.biosystemseng.2010.11.002.

Fan, B., Liu, X., Zhu, Q., Qin, G., Li, J., Lin, H., Guo, L., 2020. Exploring the interplay between infiltration dynamics and critical zone structures with multiscale geophysical imaging: a review. Geoderma 374. https://doi.org/10.1016/j.geoderma.2020.114431.

Frank, S., Tiemeyer, B., Bechtold, M., Lücke, A., Bol, R., 2017. Effect of past peat cultivation practices on present dynamics of dissolved organic carbon. Sci. Totalkl Environ. 574, 1243–1253. https://doi.org/10.1016/j.scitotenv.2016.07.121.

Frankard, P., 2004. Bilan de 12 années de gestion conservatoire des tourbières hautes dans la réserve naturelle domaniale des Hautes-Fagnes (Est de la Belgique). Géocarrefour 79, 269–276. https://doi.org/10.4000/geocarrefour.795.

Gaillardet, J., et al., 2018. OZCAR: the French network of critical zone Observatories. Vadose Zone J. 17 https://doi.org/10.2136/vzj2018.04.0067.

Hilhorst, M.A., 2000. A pore water conductivity sensor. Soil Sci. Soc. Am. J. 64, 1922–1925. https://doi.org/10.2136/sssaj2000.6461922x.

Holden, J., Chapman, P.J., Labadz, J.C., 2004. Artificial drainage of peatlands: hydrological and hydrochemical process and wetland restoration. Prog. Phys. Geogr. Earth Environ. 28, 95–123. https://doi.org/10.1191/0309133304pp403ra.

Inman, D.J., Freeland, R.S., Ammons, J.T., Yoder, R.E., 2002. Soil investigations using electromagnetic induction and ground-penetrating radar in Southwest Tennessee. Soil Sci. Soc. Am. J. 66, 206–211. https://doi.org/10.2136/sssaj2002.2060.

Jaquemart, A.L., Angenot, A., 2004. Un écosystème original, la tourbière. Le cas des tourbières acides en Belgique. Probio-revue 4.

Kettridge, N., Comas, X., Baird, A., Slater, L., Strack, M., Thompson, D., Jol, H., Binley, A., 2008. Ecohydrologically important subsurface structures in peatlands revealed by ground-penetrating radar and complex conductivity surveys. J. Geophys. Res. Biogeosci. 113 https://doi.org/10.1029/2008JG000787.

Kløve, B., Berglund, K., Berglund, O., Weldon, S., Maljanen, M., 2017. Future options for cultivated Nordic peat soils: can land management and rewetting control greenhouse gas emissions? Environ. Sci. Pol. 69, 85–93. https://doi.org/10.1016/j.envsci.2016.12.017.

Li, Y., Jonard, F., Henrion, M., Moore, A., Lambot, S., Opfergelt, S., Vanacker, V., Van Oost, K., 2024. Peat Soil Thickness and Carbon Storage in the Belgian High Fens: Insights from Multi-Sensor UAV Remote Sensing. In prep.

Lowry, C.S., Fratta, D., Anderson, M.P., 2009. Ground penetrating radar and spring formation in a groundwater dominated peat wetland. J. Hydrol. 373, 68–79. https://doi.org/10.1016/j.jhydrol.2009.04.023.

Luo, T.X.H., Lai, W., Chang, R., Goodman, D., 2019. GPR imaging criteria. J. Appl. Geophys. 165, 37–48. https://doi.org/10.1016/j.jappgeo.2019.04.008.

McCann, D.M., Culshaw, M.G., Fenning, P.J., 1997. Setting the standard for geophysical surveys in site investigation. Geol. Soc. Eng. Geol. Spec. Publ. 12, 3–34. https://doi.org/10.1144/GSL.ENG.1997.012.01.01.

McLachlan, P., Blanchy, G., Chambers, J., Sorensen, J., Uhlemann, S., Wilkinson, P., Binley, A., 2021. The application of electromagnetic induction methods to reveal the hydrogeological structure of a riparian wetland. Water Resour. Res. 57 https://doi.org/10.1029/2020WR029221.

McNeill, J., 1980. Electromagnetic Terrain Conductivity Measurement at Low Induction Numbers. Geonic Ltd, Mississauga, ON, Canada.

Minasny, B., Berglund, R., Connolly, J., Hedley, C., de Vries, F., Gimona, A., Kempen, B., Kidd, D., Lilja, H., Malone, B., McBratney, A., Roudier, P., O'Rourke, S., Rudiyanto, Padarian, J., Poggio, L., ten Caten, A., Thompson, D., Tuve, C., Widyatmanti, W., 2019. Digital mapping of peatlands – a critical review. Earth Sci. Rev. 196, 102870 https://doi.org/10.1016/j.earscirev.2019.05.014.

Minasny, B., et al., 2023. Mapping and monitoring peatland conditions from global to field scale. Biogeochemistry. https://doi.org/10.1007/s10533-023-01084-1.

Moghaddam, D., Taghizadeh-Mehrjardi, R., Triantafilis, J., 2016. Probabilistic inversion of EM38 data for 3D soil mapping in Central Iran. Geoderma Reg 7, 230–238. https://doi.org/10.1016/j.geodrs.2016.04.006.

Morishita, M., Kawahigashi, M., 2018. Heterogeneity of peat decomposition under rice cultivation on the Pacific coast. Jpn. Geoderma Reg. 12, 56–64. https://doi.org/10.1016/j.geodrs.2017.12.003.

Mormal, P., Tricot, C., 2004. Aperçu climatique des Hautes-Fagnes. Institut Royal Météorologique de Belgique.

Neal, A., 2004. Ground-penetrating radar and its use in sedimentology: principles, problems and progress. Earth Sci. Rev. 66, 261–330. https://doi.org/10.1016/j.earscirev.2004.01.004.

Parry, L.E., West, L.J., Holden, J., Chapman, P.J., 2014. Evaluating approaches for estimating peat depth. Eur. J. Vasc. Endovasc. Surg. 119, 567–576. https://doi.org/10.1002/2013JG002411.

Parsekian, A.D., Singha, K., Minsley, B.J., Holbrook, W.S., Slater, L., 2015. Multiscale geophysical imaging of the critical zone: geophysical imaging of the critical zone. Rev. Geophys. 53, 1–26. https://doi.org/10.1002/2014RG000465.

Pathirana, S., Lambot, S., Krishnapillai, M., Cheema, M., Smeaton, C., Galagedara, L., 2023. Ground-penetrating radar and electromagnetic induction: challenges and opportunities in agriculture. Remote Sens. 15, 2932. https://doi.org/10.3390/rs15112932.

Poggio, L., Gimona, A., Aalders, I., Morrice, J., Hough, R., 2020. Legacy data for 3D modelling of peat properties with uncertainty estimation in Dava bog Scotland. Geoderma Reg 22. https://doi.org/10.1016/j.geodrs.2020.e00288.

Ponziani, M., Slob, E., Ngan-Tillard, D., 2012a. Experimental validation of a model relating water content to the electrical conductivity of peat. Eng. Geol. 129-130, 48–55. https://doi.org/10.1016/j.enggeo.2012.01.011.

Ponziani, M., Slob, E., Vanhala, H., Ngan-Tillard, D., 2012b. Influence of physical and chemical properties on the low-frequency complex conductivity of peat. Near Surf. Geophys. 10, 491–501. https://doi.org/10.3997/1873-0604.2011037.

Proulx-McInnis, S., St-Hilaire, A., Rousseau, A.N., Jutras, S., 2013. A review of ground-penetrating radar studies related to peatland stratigraphy with a case study on the determination of peat thickness in a northern boreal fen in Quebec, Canada. Prog. Phys. Geogr. Earth Environ. 37, 767–786. https://doi.org/10.1177/0309133313501106.

Purvance, D.T., Andricevic, R., 2000. On the electrical-hydraulic conductivity correlation in aquifers. Water Resour. Res. 36, 2905–2913. https://doi.org/10.1029/2000WR900165.

Robinson, D.A., Lebron, I., Lesch, S.M., Shouse, P., 2004. Minimizing drift in electrical conductivity measurements in high temperature environments using the EM-38. Soil Sci. Soc. Am. J. 68, 339–345. https://doi.org/10.2136/sssaj2004.3390.

Romero-Ruiz, A., Linde, N., Keller, T., Or, D., 2018. A review of geophysical methods for soil structure characterization. Rev. Geophys. 56, 672–697. https://doi.org/10.1029/2018RG000611.

Saarikoski, H., Mustajoki, J., Hjerppe, T., Aapala, K., 2019. Participatory multicriteria decision analysis in valuing peatland ecosystem services—trade-offs related to peat extraction vs. pristine peatlands in Southern Finland. Ecol. Econ. 162, 17–28. https://doi.org/10.1016/j.ecolecon.2019.04.010.

Sass, O., Friedmann, A., Haselwanter, G., Wetzel, K.F., 2010. Investigating thickness and internal structure of alpine mires using conventional and geophysical techniques. Catena 80, 195–203. https://doi.org/10.1016/j.catena.2009.11.006.

Silvestri, S., Knight, R., Viezzoli, A., Richardson, C.J., Anshari, G.Z., et al., 2019. Quantification of peat thickness and stored carbon at the landscape scale in tropical peatlands: a comparison of airborne geophysics and an empirical topographic method. J. Geophys. Res. 124, 3107–3023.

Slater, L.D., Reeve, A., 2002. Investigating peatland stratigraphy and hydrogeology using integrated electrical geophysics. Geophysics 67, 365–378. https://doi.org/10.1190/1.1468597.

Sougnez, N., Vanacker, V., 2011. The topographic signature of quaternary tectonic uplift in the Ardennes massif (Western Europe). Hydrol. Earth Syst. Sci. 15, 1095–1107. https://doi.org/10.5194/hess-15-1095-2011.

Stroh, J.C., Archer, S., Doolittle, J.A., Wilding, L., 2001. Detection of edaphic discontinuities with ground-penetrating radar and electromagnetic induction. Landsc. Ecol. 16, 377–390.

Theimer, B.D., Nobes, D.C., Warner, B.G., 1994. A study of the geoelectrical properties of peatlands and their influence on ground-penetrating radar surveying. Geophys. Prospect. 42, 179–209. https://doi.org/10.1111/j.1365-2478.1994.tb00205.x.

Vereecken, H., et al., 2016. Modeling soil processes: review, key challenges, and new perspectives. Vadose Zone J. 15 https://doi.org/10.2136/vzj2015.09.0131.

Walter, J., Lück, E., Bauriegel, A., Richter, C., Zeitz, J., 2015. Multi-scale analysis of electrical conductivity of peatlands for the assessment of peat properties: electrical conductivity of peatlands. Eur. J. Soil Sci. 66, 639–650. https://doi.org/10.1111/ejss.12251.

Walter, J., Hamann, G., Lück, E., Klingenfuss, C., Zeitz, J., 2016. Stratigraphy and soil properties of fens: geophysical case studies from northeastern Germany. Catena 142, 112–125.

Walter, J., Lück, E., Bauriegel, A., Facklam, M., Zeitz, J., 2018. Seasonal dynamics of soil salinity in peatlands: a geophysical approach. Geoderma 310, 1–11. https://doi.org/10.1016/j.geoderma.2017.08.022.

Walter, J., Lück, E., Heller, C., Bauriegel, A., Zeitz, J., 2019. Relationship between electrical conductivity and water content of peat and gyttja: implications for electrical surveys of drained peatlands. Near Surf. Geophys. 17, 169–179. https://doi.org/10.1002/nsg.12030.

Wastiaux, C., Schumaker, R., 2003. Topographie de surface et de subsurface des zones tourbeuses des réserves naturelles domaniales des Hautes-Fagnes. In: Convention C60 entre le Ministère de la Région Wallonne, Direction générale des Ressources naturelles de l'Environnement et l'Université de Liège. Université de Liège. Unpublished report.

Wastiaux, C., Halleux, L., Schumaker, R., Streel, M., Jacqmotte, J.M., 2000. Development of the Hautes-Fagnes peat bogs (Belgium): new perspectives using groundpenetrating radar. Suo 51, 115–120.

Wende, S., Kirsch, R., 1993. Geophysical mapping of organic sediments. In: Paleolimnology of European Maar Lakes. Springer Berlin Heidelberg, pp. 109–116.

Zajıcova, K., Chuman, T., 2019. Application of ground penetrating radar methods in soil studies: a review. Geoderma 343, 116–129. https://doi.org/10.1016/j.geoderma.2019.02.024.